Quantitative Prediction of Sling Events in Turbulence at High Reynolds Numbers

Tobias Bätge [ORCID],[1,2] Itzhak Fouxon [ORCID],[3,4] and Michael Wilczek [ORCID][5,1,*]

[1]*Max Planck Institute for Dynamics and Self-Organization (MPIDS), Am Faßberg 17, 37077 Göttingen, Germany*
[2]*Faculty of Physics, University of Göttingen, Friedrich-Hund-Platz 1, 37077 Göttingen, Germany*
[3]*Department of Mechanical Engineering, Ben-Gurion University of the Negev, P.O. Box 653, Beer-Sheva 84105, Israel*
[4]*Department of Chemical Engineering, Technion, Haifa 32000, Israel*
[5]*Theoretical Physics I, University of Bayreuth, Universitätsstr. 30, 95447 Bayreuth, Germany*

Collisional growth of droplets, such as occurring in warm clouds, is known to be significantly enhanced by turbulence. Whether particles collide depends on their flow history, in particular on their encounters with highly intermittent small-scale turbulent structures, which despite their rarity can dominate the overall collision rate. Here, we develop a quantitative criterion for sling events based on the velocity gradient history along particle paths. We show by a combination of theory and simulations that the problem reduces to a one-dimensional localization problem as encountered in condensed matter physics. The reduction demonstrates that the creation of slings is controlled by the minimal real eigenvalue of the velocity gradient tensor. We use fully resolved turbulence simulations to confirm our predictions and study their Stokes and Reynolds number dependence. We also discuss extrapolations to the parameter range relevant for typical cloud droplets, showing that sling events at high Reynolds numbers are enhanced by an order of magnitude for small Stokes numbers. Thus, intermittency could be a significant ingredient in the collisional growth of rain droplets.

Until today, predicting the onset of precipitation based on cloud conditions remains a challenge [1]. A main issue is the famous "bottleneck problem"—i.e., to explain the broadening of narrow droplet size distributions produced by initial condensation of vapor on aerosol particles. The broadening is necessary to pass to the stage of rain formation where droplets collide via differential settling and coalesce to form large rain drops [2–7]. Already more than half a century ago it was proposed that cloud turbulence may contribute to rain formation by bringing similar-sized droplets together [8]. Today it is well established that as the droplets grow they pass through a range of sizes, from about 15 to 50 μm in radius, where cloud turbulence plays a significant role [2–7].

In clouds, the Reynolds number is very high [4,9]. It may reach $Re_\lambda \sim 10^4$, which means that we have to deal with a hallmark feature of developed turbulence: strong intermittency. Hence, even microscopic droplets ($\lesssim 20$ μm) with a short response time occasionally encounter extreme events of strong vorticity or strain that evolve on a comparable, "resonant" timescale. This includes regions with strong

compression in one direction. Those entrain the droplet and then disappear due to a finite lifetime, creating droplets that move along the original compression direction so fast that they detach from the flow. This leads to the formation of one-dimensional "droplet shocks" that overturn, generating regions where droplet trajectories intersect at different speeds [10–15]. As compared with smooth regions, where close droplets have similar velocities, this leads to significant enhancement in the collision rate [16], known as the "sling effect." Thus, it may foster rain formation. In fact, the rate at which sling events occur along particle trajectories is a key ingredient to the collision kernel [10,16,17]. For the sling effect to occur, turbulent velocity gradients must exceed a threshold [10] and persist for some time to have an effect. The random nature of persistence times of Navier-Stokes turbulence has not been taken into account so far, cf. [10,11,17]. Moreover, precise estimates of the sling rate as a function of the Reynolds and Stokes numbers are currently elusive [18].

Since the largest Reynolds number Re_λ attainable in today's numerical simulations is much smaller than those in clouds, a major open task is to develop quantitative criteria to predict the rate at which sling events occur and to extrapolate them to Reynolds-number ranges relevant in clouds.

In this Letter, we derive such a criterion and provide a prediction for the Re_λ dependence of the sling rate by combining theory, recent rigorous results on the high Reynolds-number limit [19], and fully resolved turbulence

simulations. Following the physical picture of one-dimensional shocks, we demonstrate that the problem of the occurrence of the sling events can be effectively reduced to a one-dimensional problem, which coincides with that of a 1D Anderson localization problem [20]. Reductions to one-dimensional models of the sling effect have been previously studied in [21–23]. We here demonstrate and numerically validate the reduction by identifying the random potential of the one-dimensional Schrödinger equation as given by the minimal real eigenvalue of the turbulent velocity gradient tensor. In the limit of small Stokes numbers $St \to 0$ and for a Gaussian random flow, sling events can be captured by an optimal fluctuation [21–23]. In a turbulent flow, we find that at $St \gtrsim 0.1$ the sling rate is determined by a whole range of characteristic values and durations of anomalously large compression.

We model droplets as inertial particles, which allows separating the effects of turbulence from more complex settings including thermodynamics and hydrodynamic interactions [4,24,25]. Already in this simple setting, the physics of particle collisions is quite rich. When the inertia of a particle is very small and its velocity relaxation to the ambient flow is fast, collision rates can be predicted in the framework of the Saffman-Turner theory, which neglects inertia. Particles are then tracers of a smooth air flow, so the trajectories of their centers never intersect. Collisions occur when finite-sized particles come so close that they geometrically overlap [8]. Particle inertia introduces fundamentally new effects such as centrifugal forces. The particles can still mostly be considered as tracers, however in an effective flow that is compressible and differs from the air flow [26,27]. Compressibility leads to preferential concentration [2,28–31], i.e., particles distribute over a multifractal attractor set in real space [32,33]. However, for particles encountering strong velocity gradients the effective tracer description fails and particles can collide due to the sling effect, i.e., the intersection of trajectories of nearby particles.

In our approach, the position $\boldsymbol{x}$ and velocity $\boldsymbol{v}$ of each particle obey [34]

$$\dot{\boldsymbol{x}}(t) = \boldsymbol{v}(t), \qquad \tau\dot{\boldsymbol{v}}(t) = \boldsymbol{u}(\boldsymbol{x}(t),t) + \boldsymbol{v}_g - \boldsymbol{v}(t). \quad (1)$$

The equations describe the relaxation of the particle velocity to the sum of the local turbulent velocity $\boldsymbol{u}(\boldsymbol{x},t)$ and the gravitational settling velocity in still air $\boldsymbol{v}_g$ with the Stokes time τ. The system can be characterized by three dimensionless parameters: the Stokes number $St = \tau\sqrt{\epsilon/\nu}$, where ϵ is the mean energy dissipation rate and ν is the kinematic viscosity, the Froude number $Fr = \epsilon^{3/4}/(g\nu^{1/4})$, where g denotes the gravitational acceleration, and the Taylor-microscale Reynolds number $Re_\lambda = \sqrt{15/(\nu\epsilon)}u^2$, where u is the rms velocity component. All these parameters influence the collisions strongly (Re_λ via the intermittency of turbulence), creating a complex problem.

For the parameter range in St and Fr considered in the following, the sling effect is concentrated in rare spatio-temporal regions that cause coexistence of three, or more, streams of particles ("folds") whose lifetime is of order τ [10]. Outside of such regions, one can then introduce a three-dimensional "particle flow" $\boldsymbol{v}(\boldsymbol{x},t)$ so that $\boldsymbol{v}(t) = \boldsymbol{v}(\boldsymbol{x}(t),t)$, i.e., the particle's velocity is uniquely defined by its position. If the flow exists, it has to obey

$$\tau(\partial_t \boldsymbol{v} + \boldsymbol{v} \cdot \nabla\boldsymbol{v}) = \boldsymbol{u} + \boldsymbol{v}_g - \boldsymbol{v} \quad (2)$$

to agree with Eqs. (1). If the evolution by this partial differential equation generates a single-valued $\boldsymbol{v}(\boldsymbol{x},t)$, the assumption is self-consistent. Conversely, if the solution becomes multivalued at some time, which implies that some of the flow derivatives blow up at that time, then $\boldsymbol{v}(\boldsymbol{x},t)$ does not exist in the blowup region. This reduces the problem to the study of the generation of finite-time blowups of velocity gradients by Eq. (2). One can see from Eq. (2) that the particle velocity gradient $P_{ik}(t) \equiv \nabla_k v_i(\boldsymbol{x}(t),t)$ evolves according to [10]

$$\tau(\dot{P} + P^2) = A - P, \quad (3)$$

where $A_{ik}(t) \equiv \nabla_k u_i(\boldsymbol{x}(t),t)$ is the fluid velocity gradient. Blowups happen if the history of gradients $A(t)$ along the particle's path $\boldsymbol{x}(t)$ produces $|P\tau| \gtrsim 1$. The P^2 term then starts to dominate in Eq. (3), producing a finite-time singularity. Crucially, the study of blowups in the matrix equation, Eq. (3), can be reduced to the study of blowups in a scalar equation, which reflects the picture of one-dimensional shocks. Note that similar scalar equations have been studied in [10,21–23]. While the reasoning towards the scalar equation presented below shares similarities to the one in [22,23], those works considered a Gaussian flow where the antisymmetric contribution of the velocity gradient tensor to the sling dynamics turns out to be negligible for $St \to 0$. In a turbulent flow, however, the sling dynamics are sensitive to vorticity, and hence, we account for the full velocity gradient tensor.

In turbulence, we observe empirically that a rare blowup event consists roughly of two stages. Initially, $P(t)$ has a typical value with $|P\tau| \ll 1$ that approximately can be set to zero in considering growth to $|P\tau| \sim 1$. Then it starts to grow according to $P\tau = \int_0^t \exp(-(t-t')/\tau)A(t')dt'$ due to the trajectory encountering a rare large A, which is persistent on the scale of τ. We take A as quasiconstant since significant oscillations would create ineffective growth of P, leading to a much smaller probability of generating a sling event. Accordingly, the matrix P grows proportionally to A, and hence commutes with it. As a result, the system can be diagonalized and the eigenvalues follow the same equation as the matrix. Once it reaches a
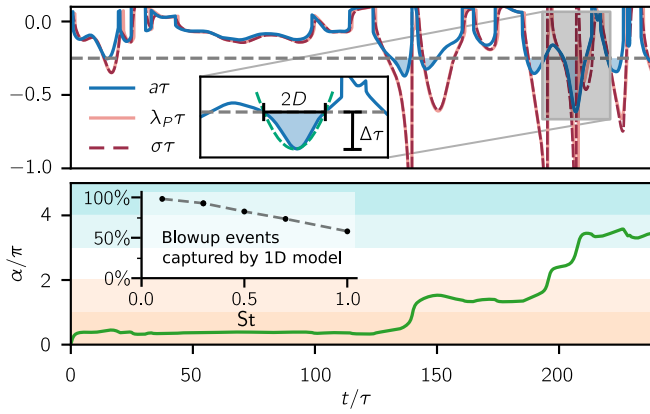
FIG. 1. Sling events along an individual trajectory in a flow with $Re_\lambda \approx 200$. The top panel shows the minimal real eigenvalue a of the sampled velocity gradient, the minimal real eigenvalue λ_P of the particle velocity gradient, which is obtained by solving the full matrix problem, Eq. (3), and its one-dimensional proxy σ, which is obtained by solving Eq. (4). Sling events correspond to the divergence of σ to negative infinity. The inset shows an excursion of a below the critical value of $-1/(4\tau)$ (gray dashed line) with duration $2D$ and depth $\Delta\tau$. Here, the green dashed line corresponds to the parabolic approximation discussed in the main text. The bottom panel shows the corresponding one-dimensional angle dynamics. Here, the sling events correspond to α crossing multiples of π. For the given trajectory with $St = 0.3$, the one-dimensional dynamics captures the occurrence of the sling events well. This is quantified in the inset, which shows the percentage of the sling events that are captured by the one-dimensional approximation, Eq. (4), compared to the full three-dimensional dynamics, Eq. (3), as a function of the Stokes number at $Re_\lambda \approx 200$.

value $P \sim 1/\tau$, Eq. (3) reduces to $\dot{P} \approx -P^2$, i.e., the evolution equation that generates a finite-time blowup of the minimal real eigenvalue $\sigma(t)$ of P. As a result, we obtain

$$\tau(\dot{\sigma} + \sigma^2) = a - \sigma, \qquad (4)$$

where $a(t)$ is the minimal real eigenvalue of the full velocity gradient tensor A, which provides a qualitatively valid description of the whole blowup process; see Supplemental Material (SM) [36] for a detailed discussion.

We can quantitatively check the validity of Eq. (4) with simulations by comparing the solutions of the full matrix equation, Eq. (3), to the one-dimensional approximation, Eq. (4). To this end, we obtained particle trajectories along with their full velocity gradient history from pseudospectral Navier-Stokes simulations [39] covering a Reynolds-number range up to $Re_\lambda \approx 500$ and taking $Fr \to \infty$, i.e., neglecting gravity; see SM [36] for more details on the parameters of our simulations.

In Fig. 1 (top), we illustrate the direct correspondence between blowup events in the full three-dimensional matrix dynamics and the one-dimensional approximation for a sample trajectory. We detect blowups as crossings

of integer multiples of π by the finite angle variable $\cot\alpha \equiv \sigma + (2\tau)^{-1}$, which avoids dealing with infinities. Figure 1 (bottom) illustrates this for the sample trajectory shown in Fig. 1 (top). Based on this, for all Reynolds numbers under consideration, we find that Eq. (4) captures blowup events in about 95% of cases for small Stokes numbers up to $St = 0.3$ whereas this percentage decreases with increasing Stokes numbers; see inset in Fig. 1 (bottom).

Having established the validity of a one-dimensional description, we can derive a quantitative criterion to predict blowups. The angle α is well-known in 1D localization problems [20] as it is related to the logarithmic derivative of the wave function ψ, which obeys the one-dimensional stationary Schrödinger equation

$$-\frac{d^2\psi}{dt^2} + \frac{a}{\tau}\psi = -\frac{\psi}{4\tau^2}; \qquad \frac{\dot{\psi}}{\psi} \equiv \sigma + \frac{1}{2\tau} = \cot\alpha. \quad (5)$$

Here, a/τ is the random "potential," $-1/(4\tau^2)$ is the "energy," and t plays the role of the spatial coordinate. The blowups of σ coincide with zeros of ψ. Most of the time the amplitude of the potential is much smaller than that of the energy and constitutes a small perturbation. This type of motion is quasiclassical and can be described by [40]

$$\psi(t) \sim \frac{\exp\left(\int^t k(s)ds\right)}{\sqrt{k(t)}}, \qquad k(t) \equiv \sqrt{\frac{1}{4\tau^2} + \frac{a(t)}{\tau}}, \quad (6)$$

where we keep only the exponentially growing solution, discarding the transients. This solution does not have zeros. One can see by inserting Eq. (6) into Eq. (5) that its validity demands that $|\dot{a}| \ll \tau k^3$. This condition is violated near the turning points in the quasiclassical region of the potential, defined by $a = -1/(4\tau)$ where the right-hand side is small. The value $a = -1/(4\tau)$ was already identified as a critical value in one-dimensional dynamics [21]. The zeros of ψ (blowups) occur in the classically allowed region where the energy $-(4\tau^2)^{-1}$ is larger than the potential a/τ and the wave function oscillates. In order to construct a globally valid solution that includes the classically allowed regions, we study rare excursions of $a(t)$ to values smaller than $-1/(4\tau)$. These excursions are typically well-separated in time so we can concentrate on the effect of one excursion that is associated with a minimum of $a(t)$ that is smaller than $-1/(4\tau)$. To obtain an analytical criterion, we perform a quadratic expansion near the minimum, which we set at $t = 0$. This leads to the Weber equation [41]

$$-\frac{d^2\psi}{dt^2} + \frac{\Delta}{D^2}t^2\psi = \Delta\psi; \qquad \frac{a}{\tau} + \frac{1}{4\tau^2} \approx -\Delta + \frac{\Delta}{D^2}t^2, \quad (7)$$

where we defined $\Delta\tau$ as the depth of excursions of $a(t)$ below the threshold $-1/(4\tau)$ and D as (half) the duration of such excursions. The inset in Fig. 1 shows such an excursion and the corresponding parabolic approximation. By solving the equation, we can construct a globally
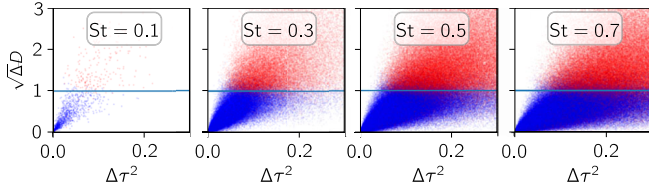
FIG. 2. Scatter plot of depth and duration of excursions of the sampled minimal eigenvalue of the velocity gradient for a Reynolds number of $Re_\lambda \approx 300$ and different Stokes numbers. The data points are plotted in red if a sling event can be identified in the corresponding one-dimensional dynamics, Eq. (4), and blue otherwise. The criterion, Eq. (8) (blue line), separates sling events from nonsling events.
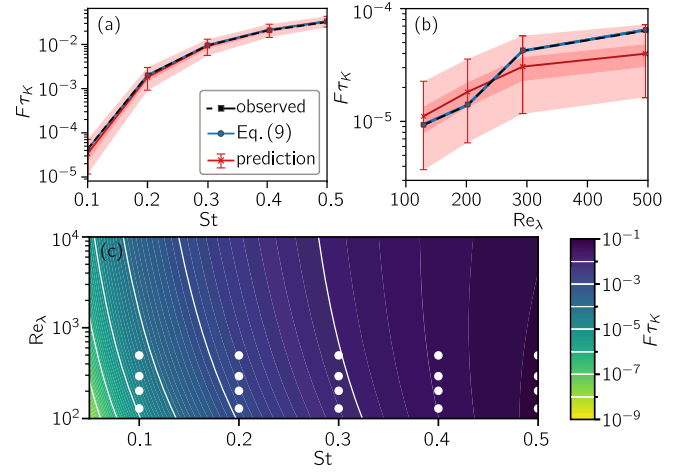

FIG. 3. Sling rate as a function of the Stokes and Reynolds number. The black dashed line in the top panels corresponds to the sling rate obtained from DNS data using the one-dimensional description; the blue line is the rhs of Eq. (9), evaluated by sampling the excursion rate and the probability that those fulfill the criterion from DNS. The red line corresponds to the prediction of the sling rate as a function of the Stokes and Reynolds number. Here, the error bars are 50% and 90% confidence intervals that are obtained by a bootstrap over the fit parameter ranges. (a) The Stokes number varies at a Reynolds number of $Re_\lambda \approx 300$. (b) The Stokes number is set to $St = 0.1$ and we vary the Reynolds number. (c) Extrapolated prediction of the sling rate as a function of St and Re_λ. The white dots mark the DNS datasets used for the extrapolation.

valid approximation for ψ; see the SM [36]. The solution demonstrates that only the quasiclassical regions with $a < -1/(4\tau)$ in between the turning points trigger blowups. The existence of the zero demands that

$$\sqrt{\Delta}D > 1. \tag{8}$$

To create a blowup, $|a(t)|$ must therefore not only become very large but also act for a sufficient time. Furthermore, if the product is also smaller than 3, ψ has only one zero, and accordingly, the excursion produces only one blowup. However, if it is between 3 and 5 then two blowups occur in a row, as the solution for ψ shows [36]. We observed both one- and two-blowup events at the considered range of Stokes numbers. The probability of three-blowup events, which would happen if the product were higher than 5, was found to be negligible for small St.

To compare this criterion to data from our direct numerical simulations (DNS), we determined the duration of the excursions and their depths from the time series of the minimal real eigenvalue $a(t)$ of the velocity gradient and solve the one-dimensional dynamics, Eq. (4). As Fig. 2 shows, our criterion, Eq. (8), indeed separates well excursions that lead to at least one sling event from those that do not. Remarkably, it even performs well for Stokes numbers as high as $St = 0.7$ where the above theory, which assumes a small probability of excursions, is not expected to work. Unfortunately, despite that Eq. (8) describes blowups of Eq. (4) at $St = 0.7$ accurately, the correspondence between full matrix dynamics and one-dimensional approach is already weak; see inset in Fig. 1. Equation (8) describes accurately about 80% of blowups of Eq. (3) at $St = 0.5$, which we propose as a heuristic upper limit of the theory. Thus, it covers the Stokes-number range of typical droplet sizes in clouds [3,4,42] where turbulence is most relevant.

Based on these findings, we can make statements about the sling rate as a function of the Reynolds number. The sling rate F can be obtained as

$$F = fP(\sqrt{\Delta}D > 1), \tag{9}$$

i.e., the rate f of excursions of $a(t)$ below $-1/(4\tau)$ times the conditional probability that the excursion obeys the criterion, Eq. (8), given that it reaches below $-1/(4\tau)$. Using the observed f, D, and Δ along trajectories from our DNS, we demonstrate the validity of the above equation in Fig. 3 as a function of the Stokes and Reynolds number. Across the range of Stokes and Reynolds numbers investigated here, we find excellent quantitative agreement.

To turn Eq. (9) into a prediction for the sling rate F, which can also be extrapolated to higher Reynolds numbers, we need to characterize the rate of excursions f, the probability of excursions leading to sling events, and their dependence on Re_λ and St. The excursion rate is the fraction of time spent below the threshold value divided by the average duration of the individual excursions:

$$f = \frac{1}{2\langle D \rangle} \int_{-\infty}^{-(4\tau)^{-1}} p(a)da, \tag{10}$$

where $p(a)$ is the probability density function (PDF) of $a(t)$. The integral above is the probability of excursions. We expect it to increase with the Reynolds number due to intermittency. In contrast, $\langle D \rangle$, which is (half) the average duration of excursions, should be approximately Reynolds number independent (but dependent on the Stokes number). For the average duration and its Reynolds number independence, we make a phenomenological argument. The inverse of the

threshold value $-1/(4\tau)$ defines a timescale that is proportional to St and independent of Re_λ. We expect the characteristic timescale for excursions to behave similarly and find $\langle D \rangle \approx 2.52 \, St\tau_K$, see SM [36], where τ_K denotes the Kolmogorov timescale.

To evaluate the integral, we note that for large negative fluctuations of $a(t)$, $\nu a^2(t)$ should be approximately proportional to the local dissipation rate. Therefore, we anticipate that the relevant left tail of $p(a)$ is directly related to the right tail of the PDF of the dissipation rate, which was observed to be log-normal in very good approximation [19]. The log-normal approximation should therefore also work well for $p(a)$. One can validate this by using large-deviation theory and our DNS results, where Re_λ is the corresponding large parameter. Because of the log-normal approximation for $p(a)$, the integral in Eq. (10) can be evaluated analytically and features an explicit dependence on Re_λ and St; for more details, we refer to the SM [36].

Finally, we turn to the probability $P(\sqrt{\Delta}D > 1)$. For reasons similar to those for $\langle D \rangle$, we expect it to have only a weak Reynolds number dependence [36]. This is confirmed by our DNS data. To fix the Stokes number dependence, it is useful to observe that $P(\sqrt{\Delta}D > 1)$ is well-defined for any St and study its behavior at $0 < St < \infty$. In the limit $St \to 0$, this probability goes to zero, since the average duration tends to zero for $St \to 0$ requiring infinitely deep excursions. In the limit $St \to \infty$, it is a finite number that gives the probability that an excursion of a below zero obeys Eq. (8). Since $P(\sqrt{\Delta}D > 1)$ is expected to grow with St monotonously, this suggests that it can be captured by a sigmoid function with two parameters controlling its amplitude and steepness. This is confirmed in the SM [36].

Above, we described how to characterize all the relevant terms in Eq. (9). The result is a quantitative description of the sling rate and its dependence on Re_λ and St (see SM [36] for an explicit formula). Equipped with this, we can fit our results as a function of the Reynolds and Stokes numbers. In Fig. 3, we show that this fit reproduces the observed sling rates in good approximation. Importantly, these fits allow an extrapolation of the results to higher Reynolds numbers as relevant in clouds. The extrapolation of our prediction in Fig. 3 shows that the effect of high Reynolds numbers becomes appreciable for lower Stokes numbers. For $St = 0.1$ and $Re_\lambda = 10^4$, our extrapolation predicts $F\tau_K \approx 2 \times 10^{-4}$, an increase of roughly an order of magnitude compared to the value at $Re_\lambda \approx 300$. The stronger Reynolds number dependence of the sling effect for small Stokes numbers might cause it to become a dominant mechanism of droplet growth in clouds also for small droplets. A precise prediction, however, about the collisions for a given sling rate requires future research about the timescale and spatial extent of sling events and their respective dependence on Re_λ.

In summary, we introduced a combined theoretical and computational approach to quantifying the sling rate that can be extrapolated to large Re_λ. This enables predictions at high Re_λ of clouds, inaccessible to simulations in the near future, for typical cloud droplets ($< 20 \, \mu m$). We confirmed the theory (valid also with gravity) through simulations of sling dynamics in turbulence, which qualitatively hold down to $Fr \sim 1$. Future studies are to include gravity computationally and provide the full formula for the collision kernel of the cloud droplets theoretically.

---

[*]michael.wilczek@uni-bayreuth.de

[1] W. W. Grabowski, H. Morrison, S.-I. Shima, G. C. Abade, P. Dziekan, and H. Pawlowska, Bull. Am. Meteorol. Soc. **100**, 655 (2019).

[2] R. A. Shaw, Annu. Rev. Fluid Mech. **35**, 183 (2003).

[3] H. Pruppacher and J. Klett, *Microphysics of Clouds and Precipitation*, Atmospheric and Oceanographic Sciences Library Vol. 18 (Springer Netherlands, Dordrecht, 2010).

[4] B. J. Devenish, P. Bartello, J.-L. Brenguier, L. R. Collins, W. W. Grabowski, R. H. A. IJzermans, S. P. Malinowski, M. W. Reeks, J. C. Vassilicos, L.-P. Wang, and Z. Warhaft, Q. J. R. Meteorol. Soc. **138**, 1401 (2012).

[5] W. W. Grabowski and L.-P. Wang, Annu. Rev. Fluid Mech. **45**, 293 (2013).

[6] A. Pumir and M. Wilkinson, Annu. Rev. Condens. Matter Phys. **7**, 141 (2016).

[7] A. P. Khain and M. Pinsky, *Physical Processes in Clouds and Cloud Modeling* (Cambridge University Press, Cambridge, England, 2018).

[8] P. G. Saffman and J. S. Turner, J. Fluid Mech. **1**, 16 (1956).

[9] S. Risius, H. Xu, F. Di Lorenzo, H. Xi, H. Siebert, R. A. Shaw, and E. Bodenschatz, Atmos. Meas. Tech. **8**, 3209 (2015).

[10] G. Falkovich, A. Fouxon, and M. G. Stepanov, Nature (London) **419**, 151 (2002).

[11] M. Wilkinson and B. Mehlig, Europhys. Lett. **71**, 186 (2005).

[12] J. Bec, L. Biferale, M. Cencini, A. S. Lanotte, and F. Toschi, J. Fluid Mech. **646**, 527 (2010).

[13] G. P. Bewley, E.-W. Saw, and E. Bodenschatz, New J. Phys. **15**, 083051 (2013).

[14] S. Lee and C. Lee, Sci. Rep. **13**, 181 (2023).

[15] J. Bec, K. Gustavsson, and B. Mehlig, arXiv:2304.01312.

[16] M. Voßkuhle, A. Pumir, E. Lévêque, and M. Wilkinson, J. Fluid Mech. **749**, 841 (2014).

[17] G. Falkovich and A. Pumir, J. Atmos. Sci. **64**, 4497 (2007).

[18] A. Bhatnagar, V. Pandey, P. Perlekar, and D. Mitra, Philos. Trans. R. Soc. A **380**, 20210086 (2022).

[19] I. Fouxon and C. Lee, Phys. Rev. E **101**, 061101(R) (2020).

[20] I. M. Lifshits, S. A. Gredeskul, and L. A. Pastur, *Introduction to the Theory of Disordered Systems* (Wiley, New York, 1988).

[21] S. A. Derevyanko, G. Falkovich, K. Turitsyn, and S. Turitsyn, J. Turbul. **8**, N16 (2007).

[22] J. Meibohm, V. Pandey, A. Bhatnagar, K. Gustavsson, D. Mitra, P. Perlekar, and B. Mehlig, Phys. Rev. Fluids **6**, L062302 (2021).

[23] J. Meibohm, K. Gustavsson, and B. Mehlig, Phys. Rev. Fluids **8**, 024305 (2023).

[24] I. Saito and T. Gotoh, New J. Phys. **20**, 023001 (2018).

[25] X.-Y. Li, A. Brandenburg, G. Svensson, N. E. L. Haugen, B. Mehlig, and I. Rogachevskii, J. Atmos. Sci. **77**, 337 (2020).

[26] M. R. Maxey, J. Fluid Mech. **174**, 441 (1987).

[27] E. Balkovsky, G. Falkovich, and A. Fouxon, Phys. Rev. Lett. **86**, 2790 (2001).

[28] S. Sundaram and L. R. Collins, J. Fluid Mech. **335**, 75 (1997).

[29] L. I. Zaichik and V. M. Alipchenkov, New J. Phys. **11**, 103018 (2009).

[30] P. J. Ireland, A. D. Bragg, and L. R. Collins, J. Fluid Mech. **796**, 617 (2016).

[31] A. J. Petersen, L. Baker, and F. Coletti, J. Fluid Mech. **864**, 925 (2019).

[32] J. Bec, J. Fluid Mech. **15**, L81 (2003).

[33] I. Fouxon, Phys. Rev. Lett. **108**, 134502 (2012).

[34] The equations apply for all droplets sizes of interest provided that τ is considered as effective time, see e.g. [35].

[35] I. Fouxon, Y. Park, R. Harduf, and C. Lee, Phys. Rev. E **92**, 033001 (2015).

[36] See Supplemental Material at http://link.aps.org/supplemental/10.1103/PhysRevLett.131.054001 for details on the general solution of ψ (Sec. S1), the analogy to the 1D localization problem (Sec. S2), parameter values for our prediction of the sling rate (Sec. S3), and the simulation setup (Sec. S4), and which includes additional Refs. [37,38].

[37] M. Abramowitz and I. A. Stegun, *Handbook of Mathematical Functions with Formulas, Graphs, and Mathematical Tables* (U.S. Government Printing Office, Washington, D.C., 1964).

[38] G. Falkovich, K. Gawędzki, and M. Vergassola, Rev. Mod. Phys. **73**, 913 (2001).

[39] C. C. Lalescu, B. Bramas, M. Rampp, and M. Wilczek, Comput. Phys. Commun. **278**, 108406 (2022).

[40] L. D. Landau and E. M. Lifshitz, *Quantum Mechanics: Non-Relastivistic Theory*, 3rd ed. (Elsevier, New York, 2013).

[41] H. Weber, Math. Ann. **1**, 1 (1869).

[42] O. Ayala, B. Rosa, L.-P. Wang, and W. W. Grabowski, New J. Phys. **10**, 075015 (2008).